Journal of Applied Polymer Science

WILEY

Applied Polymer SCIENCE

RESEARCH ARTICLE

The Investigation on Effect of the Curing Temperature on the Properties of Poly(Silylene Arylacetylene)

Ziang Wang[1] | Shuaikang Lv[2] | Liqiang Wan[1] | Farong Huang[1]

[1]Key Laboratory of Specially Functional Polymeric Materials and Related Technology (Ministry of Education), School of Materials Science and Engineering, East China University of Science and Technology, Shanghai, China | [2]Zhengzhou Hollowlite Materials Co., Ltd, Zhengzhou, China

Correspondence: Liqiang Wan (wanliqiang@163.com)

Received: 20 June 2025 | **Revised:** 12 August 2025 | **Accepted:** 18 August 2025

Funding: This work was supported by Fundamental Research Funds for the Central Universities, JKD01251701.

Keywords: composites | resins | thermal properties

ABSTRACT

Poly(silylene arylacetylene) (PSA) resins serve as a heat-resistant resin matrix and can be used for functional materials such as wave transmission and ablation materials. In this work, the relationship between the curing temperature and properties of a poly(dimethylsiliylene ethynylenephenyleneethynylene) (PSA-M) resin was investigated. The curing degree of the cured PSA-M resins was characterized by the acetylene groups content. The porosity, density, water uptake, mechanical properties, and thermal stability of the cured PSA-M resins with various curing degrees were investigated. The results reveal that the properties of the cured PSA-M resins change obviously as the curing temperature increases. With the curing temperature increasing, the density of the cured PSA-M resins decreases a little and then obviously increases. The flexural strengths of cured PSA resins gradually decrease and then reach a stable value, while the flexural moduli first decrease slightly and then increase for the cured PSA-M resins with the increase in the curing temperature. When the curing degree arrives at a certain extent, the coefficient of thermal expansion of the cured PSA-M resins tends to remain stable from room temperature to 450°C.

1 | Introduction

High-performance polymer materials have always been research hotspots in the aerospace field [1–4]. Poly(silylene arylacetylene) (PSA) resins composed of [—Si—C≡C—Ar—C≡C—] units have attracted much attention due to their excellent thermal stability, low thermal conductivity, good mechanical properties, and low dielectric constant [5–7]. Our group has been dedicated to investigating the relationship between structures and properties of PSA resins [8–10]. Specifically, we have found that modifying the substituents on the silicon atoms can enhance the processing windows of PSA resins [5]. Furthermore, the presence of dendritic structures substantially elevates the flexural modulus of the cured resins to 12.6 GPa [9] due to their hyperbranched topology. Such structures concurrently broaden processing windows by reducing melt viscosity prior to gelation. Similarly, arylether-functionalized PSA variants (PSEA) [11] demonstrate synergistically improved processability. The flexible ether linkages suppress premature crosslinking during processing, enabling extended molding cycles while elevating flexural strength to 68.4 MPa, which is critical for ablation-resistant composites requiring thermal-fatigue resistance. Notably, fluorinated-PSA systems incorporating perfluorocyclobutyl (PFCB) units [12] achieve ultralow dielectric constants (2.45–2.81) with retained thermal stability over 550°C, positioning them as benchmark wave-transparent matrices. Hybrids like 2,5-diphenyl-[1,3,4]-oxadiazole-modified PSAs [4] and polydimethylsiloxane-co-poly(silylene acetylenearyleneacetylene) [13] further exemplify property customization, where rigid heterocycles enhance char yield (> 80% at 800°C) for extreme thermal environments. These findings underscore the high potential of PSA resins for advanced aerospace applications.

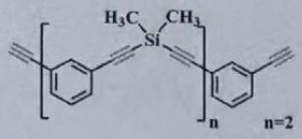

FIGURE 1 | The chemical structure of PSA-M resin. [Color figure can be viewed at wileyonlinelibrary.com]

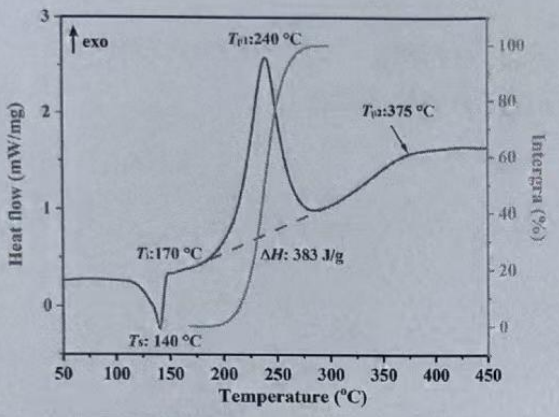

FIGURE 2 | DSC curve of PSA-M resin. [Color figure can be viewed at wileyonlinelibrary.com]

The correlation between curing degree and the properties of thermosetting resins has been extensively investigated [14–17]. Various studies have demonstrated that increasing the curing degree can lead to significant improvements in the performance of resins. For instance, Liao et al. [18] enhanced the thermal stability of phthalonitrile resins by increasing the curing temperature, resulting in a notable elevation of the temperature at 5% weight loss (T_{d5}) from 446°C to 494°C. Similarly, Zhu et al. [19] increased the curing degree of a poly(arylene ether nitrile) membrane by boosting the content of the nitrile group, ultimately reducing water uptake and enhancing dimensional stability. Xu et al. [20] increased the curing degree of epoxy asphalt by extending the curing time, leading to a substantial improvement in tensile strength. Furthermore, Liu et al. [21] elevated the glass transition temperature of phthalonitrile resins by raising the curing temperature. These findings demonstrate that the properties of thermosetting resins can be enhanced by increasing the curing degree.

When the curing temperature reaches 250°C, some acetylene groups still remain in the cured PSA resins [5]. The residual acetylene groups would affect the oxidation resistance and mechanical properties of the cured PSA resins. However, the relationship between the curing degree and properties of PSA resins has not been reported yet. Thus, we synthesized a poly(dimethylsiliylene ethynylenephenyleneethynylene) (PSA-M) resin from 1,3-diethynylbenzene and dichlorodimethylsilane based on our previously published method [5]. The chemical structure of PSA-M resin is shown in Figure 1. A series of cured PSA-M resins with various curing degrees have been obtained by increasing the curing temperature. The curing degrees of the cured PSA-M resins were characterized by the content of acetylene groups. Furthermore, the density, flexural properties, thermomechanical properties, and thermal stability of the cured PSA-M resins were investigated. Moreover, the flexural properties and interlaminar shear strengths of T300 carbon fiber-reinforced PSA-M composites at different curing temperatures were prepared and characterized. Furthermore, the relationship between the crosslinked structure and properties of the cured PSA-M resins is discussed.

This study aims to systematically investigate the effect of curing temperature on the crosslinking behavior, thermal stability, and mechanical properties of poly(dimethylsiliylene ethynylenephenyleneethynylene) (PSA-M) resins and their carbon fiber-reinforced composites. Specifically, the curing degree via residual acetylene group content was characterized to demonstrate how progressive curing temperatures (170°C–450°C) influence the density, porosity, water uptake, flexural properties, impact strength, thermomechanical behavior, and thermal stability of the cured resins. The relationship between curing-induced structural changes (e.g., interlayer distance, pore formation) and these properties was characterized. Furthermore, the corresponding effects on the flexural strength, modulus, and interlaminar shear strength of T300 carbon fiber composites were evaluated.

2 | Experimental

2.1 | Materials

PSA-M resin was synthesized from 1,3-diethynylbenzene (m-DEB) and dichlorodimethylsilane (DCMS) with the molar ratio of [m-DEB]/[DCMS] of 3/2 according to the literature in our lab. The plain carbon fiber cloth (T300, Toray) was purchased from Tianniao Co. Ltd., China.

2.2 | Preparation of Cured PSA-M Resins

The curing procedure of PSA-M resin was determined by DSC analysis. There is an endothermic peak and two exothermic peaks in the DSC curve, as shown in Figure 2. The endothermic peak at 140°C is attributed to the softening of PSA-M resin. The two exothermic peaks correspond to the curing reactions of PSA-M resin. The exothermic peak at 240°C is caused by the curing reactions among terminal acetylene (C≡C—H) groups and internal acetylene (—C≡C—) groups. The exothermic peak at 375°C is due to the curing reactions of the internal acetylene (—C≡C—) group [22]. Since the initial temperature of the exothermic peak is 170°C, the initial curing temperature was determined to be 170°C. Moreover, to avoid the highly reactive terminal acetylene groups remaining, the curing temperature of PSA-M resin should reach 250°C. The reaction temperature of the residual internal acetylene groups is above 300°C for further crosslinking. Therefore, the further curing temperature was chosen from 300°C to 450°C for the internal acetylene groups. Here, we designed the following thermal curing procedure: 170°C/2 h + 210°C/2 h + 250°C/4 h + 300°C/2 h + 350°C/2 h + 400°C/2 h + 450°C/2 h. The cured PSA-M resins were prepared by increasing the

curing temperature step by step. The cured PSA-M resins were named as cPSA-T resins (T is the curing temperature). The detailed preparation process of cPSA-T resins was as follows. A stainless-steel mold containing PSA-M resin was placed in a vacuum oven at 160°C for 0.5 h to remove residual solvent. PSA-M resin was thermally cured by the following procedure: 170°C/2 h + 210°C/2 h + 250°C/4 h. The cured resins (cPSA-170, cPSA-210, and cPSA-250) were obtained after cooling to room temperature. Then, cPSA-300, cPSA-350, cPSA-400, and cPSA-450 were obtained by heating the cPSA-250 in N_2, following this procedure: 300°C/2 h + 350°C/2 h + 400°C/2 h + 450°C/2 h. The following specimen sizes are $80 \times 15 \times 4\,mm^3$ for flexural strength, $35 \times 6 \times 2\,mm^3$ for dynamic thermomechanical analysis (DMA), and $25 \times 4 \times 4\,mm^3$ for thermomechanical (TMA) analysis.

2.3 | Preparation of Carbon Fiber-Reinforced cPSA-T (CF/cPSA-T) Composites

Twelve 12 layers of T300 carbon fiber cloths of $10 \times 15\,cm^2$ were put into a 450°C tubular furnace filled with N_2 for 5 h to remove the sizing agent on the fiber. A solution was prepared by dissolving PSA-M resin in THF and used to impregnate the treated T300 carbon fiber cloths. The impregnated cloths were air-dried to obtain the carbon fiber cloth prepregs. The prepregs were placed into a metal mold and subjected to hot-pressing under a pressure of 4.0 MPa. The thermal procedure was as follows: 170°C for 2 h, 210°C for 2 h, and 250°C for 4 h. After being naturally cooled, the composite was taken out of the mold and named CF/cPSA-250. The content of resin was around 30 wt% in the composite. Then, CF/cPSA-300, CF/cPSA-350, CF/cPSA-400, and CF/cPSA-450 were obtained step by step by heating the CF/cPSA-250 under N_2, following the step procedure: 300°C for 2 h, 350°C for 2 h, 400°C for 2 h, and 450°C for 2 h. The following specimen sizes are $45 \times 15 \times 2\,mm^3$ for flexural property test and $20 \times 10 \times 2\,mm^3$ for interlaminar shear strength test.

2.4 | Characterization

Differential scanning calorimetry (DSC) analysis was performed with the Q2000 analyzer (TA, USA) with a heating rate of $10°C \cdot min^{-1}$. Fourier-transform infrared (FT-IR) spectra were collected at room temperature on a Nicolet iS10 infrared spectrometer (Thermo Scientific, USA). X-ray diffraction patterns (XRD) were recorded on a Rigaku D/Max 2550 VB/PC (Rigaku, Japan) rotating anode x-ray diffractometer at room temperature. The Brunner-Emmet-Teller (BET) measurements were conducted on a 3Flex adsorption analyzer (Micromeritics, USA) by nitrogen adsorption. Thermal gravimetric analysis (TGA) was conducted on a TGA/DSC 1LF analyzer (Mettler Toledo, Switzerland) with a $10°C \cdot min^{-1}$ heating rate. DMA was conducted on a DMA 1 mechanical analyzer (Mettler Toledo, Switzerland) in N_2 with a heating rate of $10°C \cdot min^{-1}$. TMA was performed with an L75VS 2000C instrument (Linseis, Germany) in the air with a heating rate of $5°C \cdot min^{-1}$. The mechanical properties of cured resins and composites were measured on a CMT 4204 universal testing machine (SANS, China) at a speed of $2\,mm \cdot min^{-1}$. The field-emission scanning electron microscope (SEM) image was recorded on S-4800 (Hitachi, Japan). The density was measured by a ME204E density balance (Mettler Toledo, Switzerland) at room temperature.

The porosity (P) was measured by placing cPSA-T resins (bulk) in boiling water for 2 h and calculated by the following Equation (1):

$$P = \frac{m_1 - m_0}{m_1 - m_2} \tag{1}$$

where m_0 is the weight of cPSA-T resins in the air, m_1 is the weight of cPSA-T resins in the air after being immersed in boiling water, and m_2 is the weight of cPSA-T resins in the water after being immersed in boiling water.

The water uptake was measured by placing cPSA-T resins (bulk) in the water at room temperature and calculated by the following Equation (2):

$$W = \frac{m_1 - m_0}{m_0} \times 100\,\% \tag{2}$$

where W is the water uptake of cPSA-T resins, m_0 and m_1 are the weights of cPSA-T resins before and after being immersed in the water at room temperature for a period of time.

3 | Results and Discussion

3.1 | The Curing Degree of cPSA-T Resins

The curing degree of cPSA-T resins was characterized by FT-IR spectroscopy. The FT-IR spectra of PSA-M and cPSA-T resins are shown in Figure 3a. With the curing temperature increasing, the vibration peak of C≡C—H at $3298\,cm^{-1}$ almost disappears at 300°C, and the vibration peak of —C≡C— at $2150\,cm^{-1}$ gradually weakens. Since Si—CH_3 groups do not involve in the curing reaction, [23] the vibration peak of Si—CH_3 at $1250\,cm^{-1}$ remains unchanged. With the curing temperature increasing, the decrease in the content of acetylene groups indicates the increase of the curing degree of cPSA-T resins. Therefore, the curing degree of cPSA-T resins was characterized by the content of acetylene groups in cPSA-T resins. It is noted that the designed and synthesized PSA resin contains a total of six acetylene groups, including two terminal acetylene groups and four internal acetylene groups. Hence, the content of acetylene (C_a) groups of cPSA-T resins was calculated as the following Equations (3–5).

$$C_a = \frac{2C_{ia}}{6} + \frac{4C_{ia}}{6} \tag{3}$$

$$C_{ia} = \frac{(A_{ia}/A_r)_{cPSA-T}}{(A_{ia}/A_r)_{PSA-M}} \tag{4}$$

$$C_{ia} = \frac{(A_{ia}/A_r)_{cPSA-T}}{(A_{ia}/A_r)_{PSA-M}} \tag{5}$$

where C_{ta} is the content of the terminal acetylene groups of cPSA-T resins, C_{ia} is the content of the internal acetylene groups of cPSA-T resins, A_{ta} is the integrated intensity of the peak of terminal acetylene groups for PSA-M or cPSA-T resins in FT-IR spectra, A_{ia} is the integrated intensity of the peak of internal acetylene groups of PSA-M or cPSA-T resins in FT-IR spectra, and A_r is the integrated intensity of the peak of Si—CH_3 of PSA-M or cPSA-T resins in FT-IR spectra. Thus, the curing degree (D_c) of cPSA-T resins is determined by Equation (6).

$$D_c = 1 - C_a \tag{6}$$

The content of acetylene groups and the curing degree of cPSA-T resins are listed in Table S1. Figure 3b illustrates the relationship between the curing procedure and the curing degree. Notably, the content of internal acetylene groups in cPSA-T resins begins to significantly decrease at the step of 350°C. Meanwhile, cPSA-450 has almost no residual internal acetylene groups. This indicates that the internal acetylene groups react obviously with each other at above 300°C.

3.2 | The Structures of cPSA-T Resins

3.2.1 | XRD Patterns of cPSA-T Resins

X-ray diffraction analysis was utilized to determine the interlayer distance of the crosslinked network for PSA-M and cPSA-T resins, as depicted in Figure 4a. Compared to the PSA-M resin, the cPSA-T resins exhibit wide diffraction peaks with low intensity. The diffraction peaks of cPSA-170, cPSA-210, cPSA-250, and cPSA-300 appear at $2\theta = 18.6°$, 18.3°, 18.2°, and 18.1°, respectively. However, the diffraction peaks of cPSA-350, cPSA-400, and cPSA-450 show a broad peak almost close to the background. This indicates that the interlayer distance of the crosslinked network gradually increases with the curing temperature from 170°C to

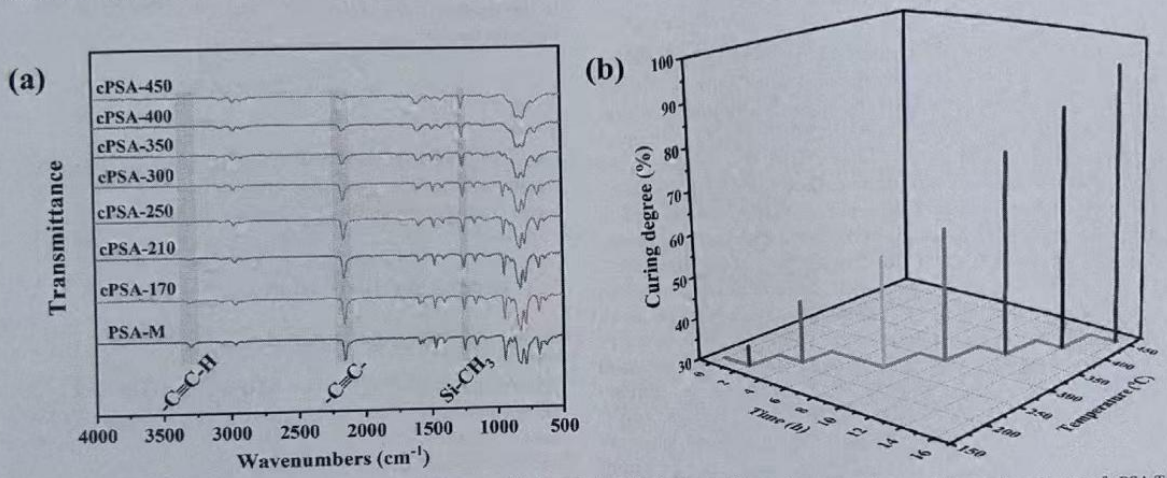

FIGURE 3 | (a) FT-IR spectra of PSA-M and cPSA-T resins, (b) the relationship between the curing procedure and the curing degree of cPSA-T resins. [Color figure can be viewed at wileyonlinelibrary.com]

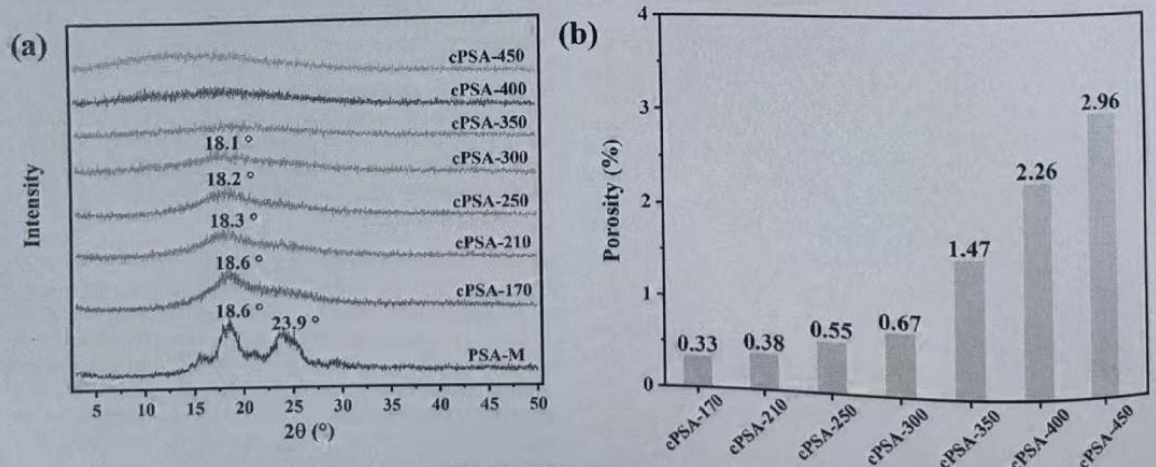

FIGURE 4 | (a) XRD patterns of the cPSA-T and PSA-M resins, (b) the porosities of cPSA-T resins. [Color figure can be viewed at wileyonlinelibrary.com]

300°C. The terminal acetylene groups of the PSA-M resin mainly form the polyene structures (−C=C−C=C−C=C−) at 170°C [24]. With the curing temperature increasing, the curing reactions mainly involve the Diels-Alder reaction among Ph−C≡C, C≡C, and −C=C−C=C− groups and the cyclotrimerization of C≡C groups [25]. Consequently, the crosslinked structure of the cPSA-T resins transitions from polyene to aromatic ring (e.g., benzene ring and naphthalene ring) with the increase of curing temperature. Additionally, the Van der Waals volume of aromatic rings is higher than that of polyene structures [26]. Therefore, the crosslinked network of cPSA-170 is a tighter stacking than that of cPSA-300. When the curing temperature is between 350°C and 450°C, the crosslinked network of cPSA-T resins becomes more disordered due to the curing reactions of internal acetylene groups. This suggests that the crosslinked network of the cPSA-T resins is more tightly stacked when the curing temperature is above 350°C. Therefore, with the curing temperature increasing, the interlayer distance of the crosslinked network increases between 170°C and 300°C and then decreases between 350°C and 450°C.

3.3 | The Porosities of cPSA-T Resins

The porosities of cPSA-T resins are shown in Figure 4b. With the curing temperature increasing, the porosities of cPSA-T resins increase. Especially when the curing temperature is above 350°C, the porosities of cPSA-T resin increase significantly. The increase in the interlayer distance of the crosslinked network leads to the increase in the porosities of cPSA-T resins with the curing temperature from 170°C to 300°C. However, due to the presence of a large number of aromatic rings in cPSA-300, the chain segment movement of cPSA-300 becomes difficult at high temperatures. Thus, the crosslinked network contracts significantly when the curing temperature is over 350°C, resulting in the increase of pores inside cPSA-T resins. With the reaction degree of the internal acetylene groups increasing, the crosslinked network contracts more severely, and the pore size becomes larger.

3.4 | The Properties of cPSA-T Resins

3.4.1 | The Density of cPSA-T Resins

The increase in macroscopic density reflects the tight stacking of the crosslinked network for the cured resins [27]. Figure 5a demonstrates that the density of cPSA-T resins first decreases a little with the curing temperature from 170°C to 300°C and then increases with the curing temperature from 350°C to 450°C. cPSA-300 shows the lowest density (1.011 g/cm^3) and the density (1.045 g·cm^{-3}) of cPSA-450 is highest in cPSA-T resins. The large interlayer distance of the crosslinked network contributes to the decrease in the density of cPSA-T resins. Therefore, the density

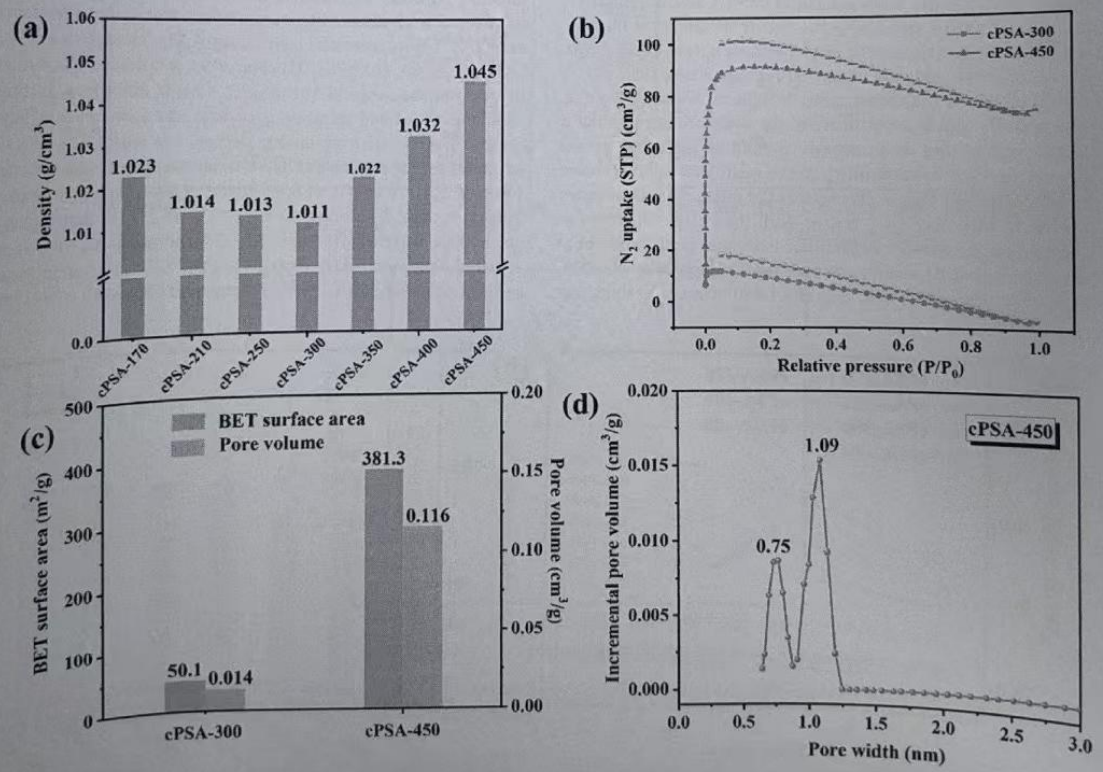

FIGURE 5 | (a) The density of cPSA-T resins, (b) N_2 adsorption–desorption curves of cPSA-300 and cPSA-450, (c) BET surface area and pore volume of cPSA-300 and cPSA-450, (d) the pore size distribution of cPSA-450. [Color figure can be viewed at wileyonlinelibrary.com]

of cPSA-T resins decreases with the curing temperature from 170°C to 300°C. When the curing temperature is above 350°C, the curing reactions of internal acetylene groups result in a contraction of the macroscopic volume. As a result, the density of cPSA-T resins increases with the curing temperature from 350°C to 450°C. The density of the cPSA-T resin decreases corresponding to the increase in porosity with the curing temperature from 170°C to 300°C. However, with the curing temperature from 350°C to 450°C, the increase in the density of cPSA-T resins would be contradictory to the increase in porosity. This may be due to the contraction of the crosslinked network being greater than the increase in porosity. In order to further characterize the pore of cPSA-T resins, we selected cPSA-300 with the lowest density and cPSA-450 with the highest density for nitrogen adsorption–desorption testing, as shown in Figure 5b. The BET surface area of cPSA-300 and cPSA-450 is 50.1 and 381.3 m^2/g, respectively, as shown in Figure 5c. The pore size distribution of cPSA-450 is shown in Figure 5d. The pore size of cPSA-300 is too small to be characterized. These results show that there are a large number of micropores in cPSA-450, even though its density is the highest in cPSA-T resins. Therefore, due to the contraction of the crosslinked network, the pore size of cPSA-T resins rises with the curing temperature from 350°C to 450°C.

3.4.2 | Water Uptake of cPSA-T Resins

Figure 6a shows the water uptake of cPSA-T resins, which exhibit an ascending trend with the curing temperature increasing. However, it is noteworthy that the water uptake of cPSA-170, cPSA-210, cPSA-250, and cPSA-300 remains below 0.5% over a period of 5 days, indicating their exceptional water resistance. The porosity and hydrophilicity of the resin are the two main factors influencing water uptake. Specifically, a higher porosity and stronger hydrophilicity in the resin lead to an increase in water uptake. Figure 6b presents the contact angle of water on the surface of cPSA-T resins. With the curing temperature increasing, the contact angle diminishes and then stabilizes at a certain value. This indicates that the hydrophilicity of cPSA-300, cPSA-350, cPSA-400, and cPSA-450 is stronger than that of cPSA-170, cPSA-210, and cPSA-250. Consequently, cPSA-350, cPSA-400, and cPSA-450 demonstrate elevated water uptake due to their combination of high porosity and strong hydrophilicity.

3.4.3 | The Mechanical Properties of cPSA-T Resins

The flexural strengths and flexural moduli of cPSA-T resins are shown in Figure 7a. With the curing temperature from 170°C to 300°C, the flexural strength decreases and the flexural modulus decreases slightly. However, when the curing temperature increases from 350°C to 450°C, the flexural strength stabilizes and the flexural modulus increases. This phenomenon can be attributed to the increase in crosslinking density of cPSA-T resins [28, 29]. Additionally, the further curing of internal acetylene groups significantly contributes to the enhancement of the flexural moduli of cPSA-T resins. Figure 7b illustrates the impact strengths of cPSA-T resins. As the curing temperature increases, the impact strength decreases and then stabilizes at approximately 1.50 kJ/m^2. The impact strength reflects the toughness of resins. Therefore, it can be inferred that the toughness of cPSA-T resins decreases with the increase in the curing temperature. This is due to the increase in rigid aromatic rings of the crosslinked structure with the curing temperature increasing.

Figure 8a presents the DMA curves of cPSA-T resins. The storage moduli of cPSA-T resins stabilize at a certain value and then increase with the increase in the curing temperature. When the curing temperature is above 350°C, the storage modulus of cPSA-T resins increases significantly. The storage moduli of cPSA-170, cPSA-210, cPSA-250, and cPSA-300 decrease and then increase in the range of 50 to 450°C. This is due to the further curing of unreacted terminal acetylene and internal acetylene groups. Due to the high curing degree, the storage moduli of cPSA-350, cPSA-400, and cPSA-450 remain a stable value in the range of 50°C to 450°C. cPSA-170 and cPSA-210 clearly display glass transition temperatures at 129°C and 176°C, respectively. In the loss tangent curve of cPSA-250, the peak at 180°C is attributed to the secondary relaxation [30]. When the curing temperature is above 300°C, the loss tangent of cPSA-300, cPSA-350,

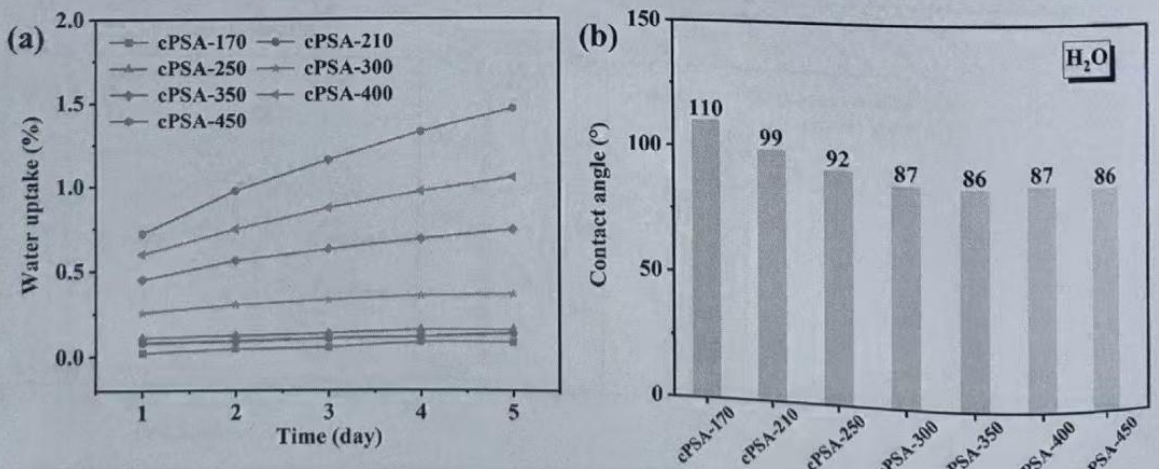

FIGURE 6 | (a) The water uptake of cPSA-T resins, (b) the contact angle of water on the surface of cPSA-T resins. [Color figure can be viewed at wileyonlinelibrary.com]

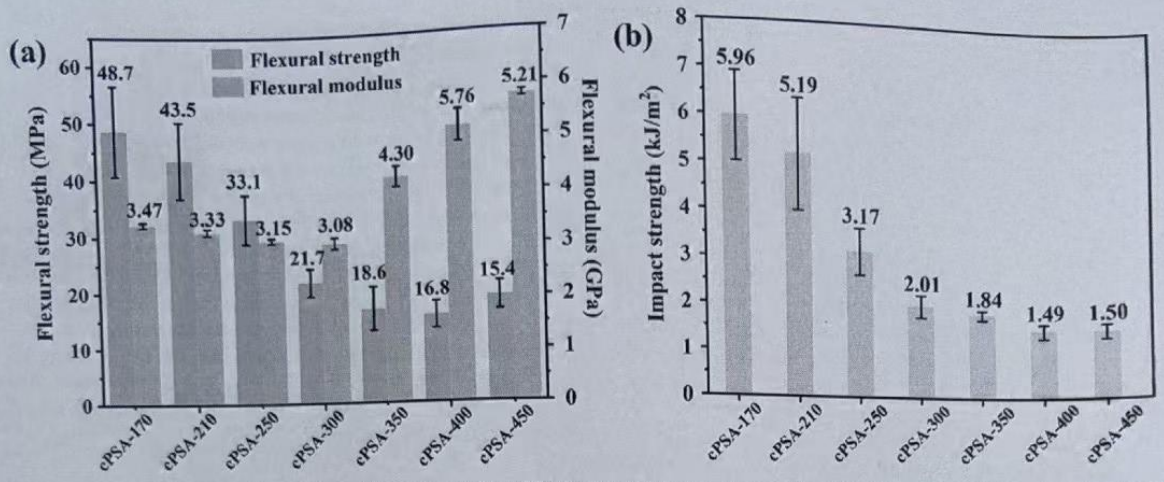

FIGURE 7 | (a) The flexural strengths and flexural moduli of cPSA-T resins, (b) the impact strengths of cPSA-T resins. [Color figure can be viewed at wileyonlinelibrary.com]

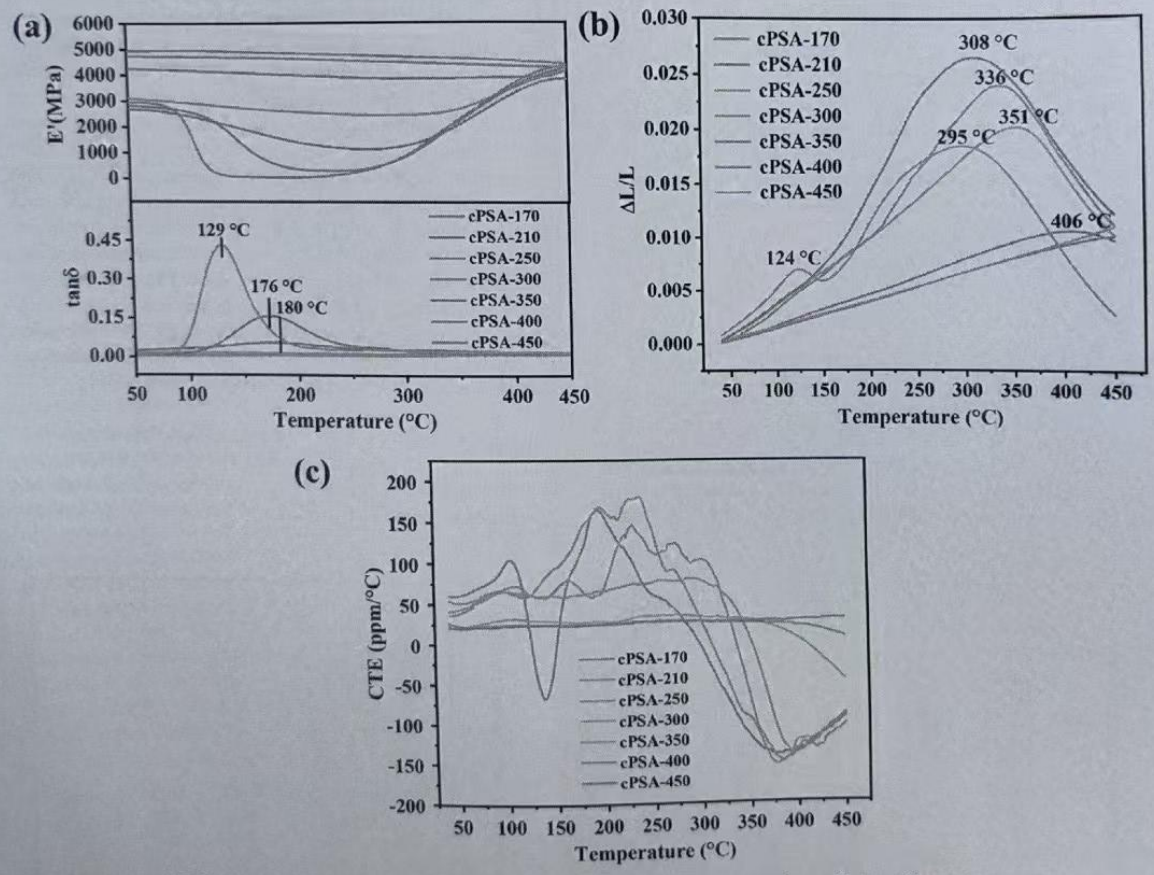

FIGURE 8 | (a) DMA curves of cPSA-T resins in N_2, (b) TMA curves of cPSA-T resins in air, (c) the coefficient of thermal expansion–temperature curves of cPSA-T resins. [Color figure can be viewed at wileyonlinelibrary.com]

cPSA-400, and cPSA-450 remains stable. These results indicate that the chain segment movement of cPSA-T resins becomes difficult with the increase in the curing degree.

The dimensional stability of cPSA-T resins was characterized by TMA from room temperature to 450°C, as shown in Figure 8b. With the temperature rising, cPSA-170, cPSA-210, cPSA-250,

cPSA-300, and cPSA-350 initially expand and then contract. The decline of dimension for cPSA-170, cPSA-210, cPSA-250, cPSA-300, and cPSA-350 is due to the further curing of unreacted terminal acetylene and internal acetylene groups. The temperature at which cPSA-T resins start to contract is referred to as T_c. The T_c values for cPSA-170, cPSA-210, cPSA-250, cPSA-300, and cPSA-350 are 295°C, 308°C, 336°C, 351°C, and 406°C, respectively. With the curing temperature increasing, the T_c shifts toward higher temperatures. Thermal expansion property is a significant thermal property that helps to determine the potential applications of a material. According to the slope of the TMA curves, the coefficient of thermal expansion (CTE) is obtained for cPSA-T resins, as shown in Figure 8c. The CTE of cPSA-170 at 210°C is higher than that at room temperature. The increase of CTE reflects the increase in the free volume of the resin. This indicates that during the curing process of cPSA-170, the free volume of the resin increases; thus, the density of the obtained cPSA-210 is lower than that of cPSA-170. Likewise, the CTE of cPSA-210 and cPSA-250 in 200°C to 300°C is higher than that at room temperature. Thus, the densities of the obtained cPSA-250 and cPSA-300 decrease in sequence. The CTE of cPSA-300, cPSA-350, and cPSA-400 remains stable and then decreases with temperature rising. This demonstrates that during the curing process of cPSA-300, cPSA-350, and cPSA-400, the free volume of the resin decreases. Consequently, the densities of the obtained cPSA-350, cPSA-400, and cPSA-450 increase in sequence. The CTE of cPSA-350, cPSA-400, and cPSA-450 is 28.5, 25.0, and 23.9 ppm/°C, respectively, which are lower than most thermoplastic and thermosetting polymers (30–100 ppm/°C) [31]. Therefore, when the curing temperature is above 350°C, the curing resins cPSA-350, cPSA-400, and cPSA-450 show stable thermomechanical properties.

3.4.4 | The Mechanical Properties of the CF/cPSA-T Composites

The flexural strengths and flexural moduli of the CF/cPSA-T composites are shown in Figure 9a. The flexural strength and flexural moduli decrease and then stabilize with the increase of the curing temperature. The flexural moduli of the CF/cPSA-T composites show a different trend compared with that of cPSA-T resins. Figure 9b shows the interlaminar shear strengths of the CF/cPSA-T composites. With the curing temperature increasing, the interlaminar shear strengths of the CF/cPSA-T composites decrease, indicating a worsening interface between the resin and the fiber with the increase in the curing temperature. Therefore, the decrease of flexural properties for CF/cPSA-T composites may be attributed to the deterioration of the interface between the carbon fiber and the resin. The interlaminar SEM images of the CF/cPSA-T composites are presented in Figure 10. The resin strongly adheres to the carbon fiber in CF/cPSA-250. However, as the curing temperature increases, the amount of resin adhered to the carbon fiber decreases. There is less resin covering the fiber in CF/cPSA-450. Consequently, the poor interface in composites at a high curing temperature leads to lower flexural properties.

3.4.5 | Thermal Stability of cPSA-T Resins

TGA was used to investigate the thermal stability of cPSA-T resins. Figure 11a illustrates the TGA curves of cPSA-T resins in N_2, and the results are summarized in Table S2. All TGA curves of cPSA-T resins are similar. The T_{d5} of cPSA-T resins is around 660°C in N_2. The result indicates that the curing temperature has minimal impact on the thermal stability of cPSA-T resins in N_2. As shown in Figure 11b, the TGA curves under air show a significant difference compared with those under N_2. The TGA curves show that the weight initially increases and then decreases rapidly in air. The weight gain observed starting at about 250°C is attributed to the oxidation of unreacted acetylene group [32]. cPSA-170, cPSA-210, and cPSA-250 show low oxidation temperature, high weight gain, and low T_{d5} due to the presence of multiple unreacted acetylene groups. These results indicate that cPSA-T resins achieve better thermal oxidative stability when the curing temperature is above 300°C.

Compared with other similar PSA resins used in wave transmission and ablation applications shown in Table S3, PSA-M resin with different curing temperatures all demonstrated outstanding thermomechanical performance, which could mainly be

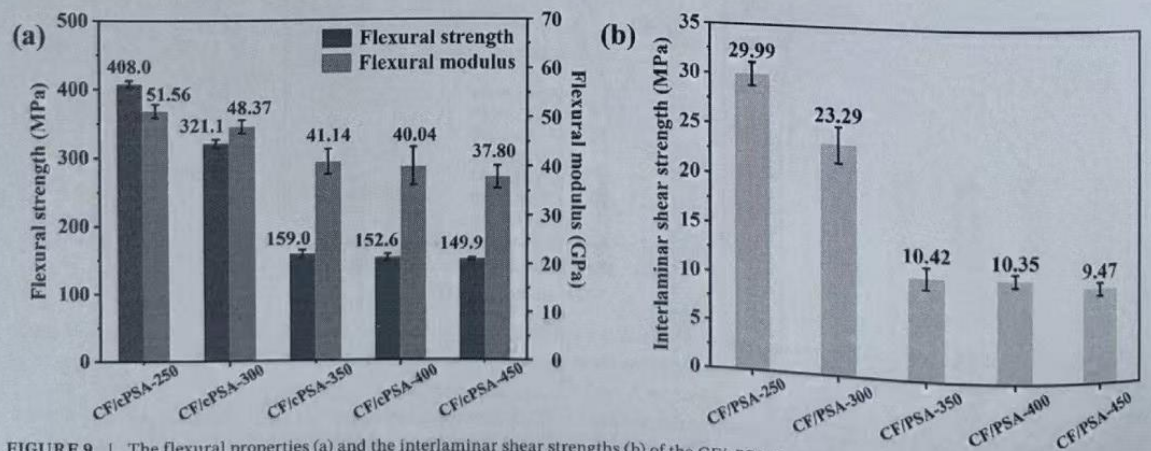

FIGURE 9 | The flexural properties (a) and the interlaminar shear strengths (b) of the CF/cPSA-T composites. [Color figure can be viewed at wileyonlinelibrary.com]

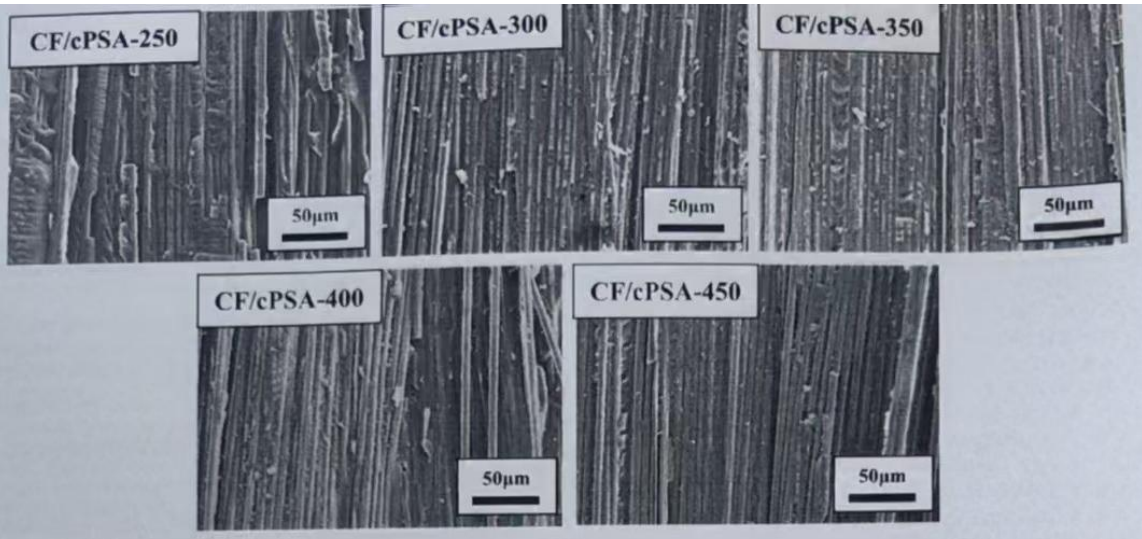

FIGURE 10 | The interlaminar SEM images of the CF/cPSA-T composites.

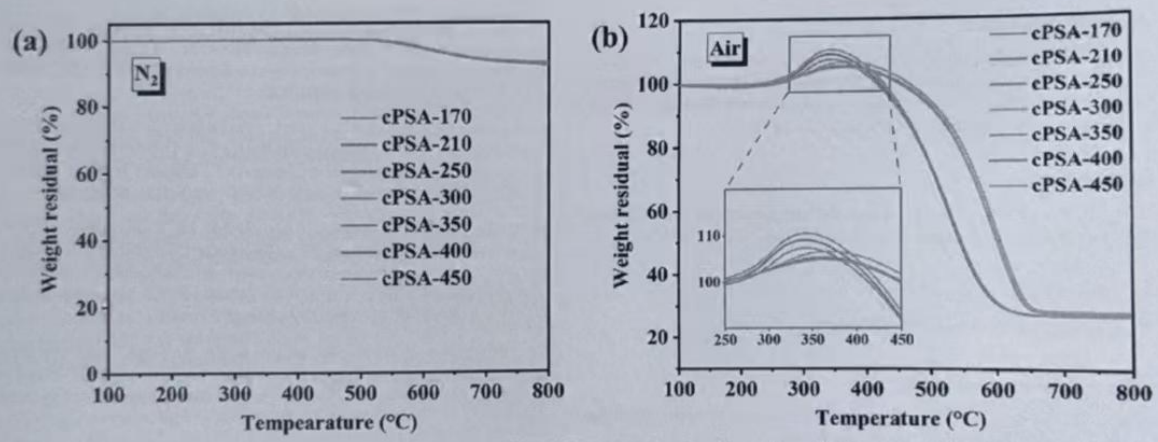

FIGURE 11 | TGA curves of cPSA-T resins in N_2 (a) and air (b). [Color figure can be viewed at wileyonlinelibrary.com]

attributed to the substitution of methyl as the side group. Unlike bulkier substituents such as phenyl, the compact methyl groups reduce steric hindrance, facilitating tighter molecular packing and higher crosslink density. Moreover, the arrangement of internal alkynes within the molecular segments is also more compact, which contrasts with arylether-modified PSAs, where flexible ether linkages introduce oxygen elements in the molecular structure.

4 | Conclusion

To investigate the relationship between curing temperature and properties of PSA-M resin, a temperature procedure was designed as follows: 170°C/2 h + 210°C/2 h + 250°C/4 h + 300 °C/2 h + 350°C/2 h + 400°C/2 h + 450°C/2 h. With the curing temperature increasing, the acetylene content of cPSA-T resins decreases, indicating the curing degree increases. Especially when the curing temperature is above 350°C, the curing degree of cPSA-350 is significantly increased compared to that of cPSA-300 due to the curing reaction between internal acetylene groups. The interlayer distance of the crosslinked network increases and then decreases with the curing temperature increasing. The porosities of cPSA-T resins increase as the curing temperature increases. The density of cPSA-T resins decreases a little and then increases with the curing temperature increasing. When the curing temperature reaches 300°C, cPSA-300 exhibits the lowest density. With the curing temperature increasing, the water uptake of cPSA-T resins increases, the flexural strengths of cPSA-T resins gradually decrease and then reach a stable value, while the flexural moduli decrease slightly and then gradually increase. cPSA-T resins with low curing degree first expand and then contract in 50°C–450°C. The flexural properties of CF/cPSA-T composites decrease and stabilize with the increase in

the curing temperature. With the curing temperature increasing, the thermal oxidative stability of cPSA-T resins increases and then remains stable. Unlike prior studies focusing on PSA modifications, this work systematically decouples the curing temperature-dependent evolution of crosslinked structures and properties for PSA-M resin, providing data support for studying the reliability of PSA resin as a high-temperature resistant material in practical application scenarios. Moreover, we found that PSA-M resin forms microporous structures at higher temperatures, which is a new discovery that we will continue to study based on about the adsorption and separation abilities.

However, under the current system, the temperature required for the complete reaction of the internal alkyne groups within PSA-M resin is excessively high; the development of a suitable catalyst remains necessary to lower the reaction temperature, thereby enabling the internal alkyne groups in PSA-M resin to achieve complete conversion at a lower temperature. Furthermore, the interfacial adhesion between T300 carbon fibers and PSA-M resin requires improvement. Further research is needed to identify suitable crosslinking agents to enhance interfacial bonding at the fiber-resin interface.

Author Contributions

Ziang Wang: data curation (lead), formal analysis (lead), writing – original draft (lead). **Shuaikang Lv:** methodology (equal). **Liqiang Wan:** investigation (lead), resources (lead). **Farong Huang:** funding acquisition (lead), writing – review and editing (lead).

Acknowledgments

The authors gratefully acknowledge the support of the Fundamental Research Funds for the Central Universities (no. JKD01251701).

Conflicts of Interest

The authors declare no conflicts of interest.

Data Availability Statement

The data that support the findings of this study are available from the corresponding author upon reasonable request.

References

1. J. Li, H. Wang, and S. Li, "A Novel Phosphorus-Silicon Containing Epoxy Resin With Enhanced Thermal Stability, Flame Retardancy and Mechanical Properties," *Polymer Degradation and Stability* 164 (2019): 36–45, https://doi.org/10.1016/j.polymdegradstab.2019.03.020.

2. D. Zhou, L. Yuan, W. Hong, H. Zhang, A. Hu, and S. Yang, "Molecular Design of Interpenetrating Fluorinated Polyimide Network With Enhanced High Performance for Heat-Resistant Matrix," *Polymer* 173 (2019): 66–79, https://doi.org/10.1016/j.polymer.2019.04.034.

3. J. Yun, L. Chen, H. Zhao, X. Zhang, W. Ye, and D. Zhu, "Boric Acid as a Coupling Agent for Preparation of Phenolic Resin Containing Boron and Silicon With Enhanced Char Yield. Macromol," *Macromolecular Rapid Communications* 40 (2018): 1800702, https://doi.org/10.1002/marc.201800702.

4. M. Ma, C. Gong, C. Li, Q. Yuan, and F. Huang, "The Synthesis and Properties of Silicon-Containing Arylacetylene Resins With Rigid-Rod 2,5-Diphenyl-[1,3,4]-Oxadiazole Moieties," *European Polymer Journal* 143 (2021): 110192, https://doi.org/10.1016/j.eurpolymj.2020.110192.

5. X. Liu, M. Ma, C. Li, J. Tang, Q. Yuan, and F. Huang, "Effect of Side Groups on the Properties of Silicon-Containing Arylacetylene Resins," *Polymer Engineering and Science* 62 (2022): 793–801, https://doi.org/10.1002/pen.25885.

6. M. Ma, N. Dai, X. Liu, C. Li, Q. Yuan, and F. Huang, "Reinforcing the Poly(Silylene Arylacetylene)s via Strong π-π Stacking Interactions," *Polymer* 229 (2021): 123976, https://doi.org/10.1016/j.polymer.2021.123976.

7. C. Gong, X. Huang, S. Lv, J. Li, J. Tang, and F. Huang, "Poly(Silylene Arylacetylene)s Containing Hexafluoroisopropylidene With Attractive Mechanical Properties and Dielectric Performance for Wave-Transparent Composites," *Materials Chemistry Frontiers* 7 (2023): 5015–5027, https://doi.org/10.1039/D3QM00584D.

8. N. Dai, J. Tang, M. Ma, X. Liu, C. Li, and F. Huang, "Star-Shaped Arylacetylene Resins Derived From Silicon," *Journal of Polymer Engineering* 40 (2020): 676–684, https://doi.org/10.1515/polyeng-2020-0083.

9. J. Luo, X. Liu, M. Ma, J. Tang, and F. Huang, "Dendritic Poly(Silylene Arylacetylene) Resins Based on 1,3,5-Triethynylbenzene," *European Polymer Journal* 129 (2020): 109628, https://doi.org/10.1016/j.eurpolymj.2020.109628.

10. J. Li, C. Gong, S. Lv, J. Tang, Q. Yuan, and F. Huang, "High-Performance Poly(Methylsilane Arylether Arylacetylene) Resins With Low Curing Temperatures and Weak Secondary Relaxations," *Journal of Applied Polymer Science* 141, no. 5 (2023): e54875, https://doi.org/10.1002/app.54875.

11. J. Li, S. Lv, C. Gong, Y. Zhou, and F. Huang, "Effect of the Linking Positions on the Benzene Ring on Properties of Poly(Silane Arylether Arylacetylene)s," *Journal of Polymer Science* 60 (2022): 3232–3243, https://doi.org/10.1002/pol.20220185.

12. C. Gong, X. Huang, J. Li, et al., "Perfluorocyclobutyl Aryl Ether-Based Poly(Silylene Arylacetylene)s With a Low Dielectric Constant for Advanced Wave-Transparent Composites," *European Polymer Journal* 181 (2022): 111655, https://doi.org/10.1016/j.eurpolymj.2022.111655.

13. X. Hu, Q. Yuan, F. Huang, Z. Liu, and B. Li, "Preparation and Ablative Behaviors of Carbon Fiber-Reinforced Polydimethylsiloxane-Co-Poly (Silylene Acetylenearyleneacetylene) Composites," *Journal of Applied Polymer Science* 139, no. 44 (2022): e53087, https://onlinelibrary.wiley.com/doi/full/10.1002/app.53087.

14. J.-F. Nguyen, B. Pomes, M. Sadoun, and E. Richaud, "Curing of Urethane Dimetracrylate Composites: A Glass Transition Study," *Polymer Testing* 80 (2019): 106113, https://doi.org/10.1016/j.polymertesting.2019.106113.

15. J. Moosburger-Will, M. Greisel, M. G. R. Sause, R. Horny, and S. Horn, "Influence of Partial Cross-Linking Degree on Basic Physical Properties of RTM6 Epoxy Resin," *Journal of Applied Polymer Science* 130 (2013): 4338–4346, https://doi.org/10.1002/app.39722.

16. X. Shi, D. Soule, Q. Ge, H. Lu, and K. Yu, "Evolution of Material Properties During the Solvent-Assisted Recycling of Thermosetting Polymers: To Reduce the Residual Stress and Material Inhomogeneity," *Materials Today Sustainability* 19 (2022): 100167, https://doi.org/10.1016/j.mtsust.2022.100167.

17. J. Moosburger-Will, M. Greisel, and S. Horn, "Physical Aging of Partially Crosslinked RTM6 Epoxy Resin," *Journal of Applied Polymer Science* 131 (2014): 41121, https://doi.org/10.1002/app.41121.

18. S. Liao, H. Wu, X. He, et al., "Promoting Effect of Methyne/Methylene Moiety of Bisphenol E/F on Phthalonitrile Resin Curing: Expanding the Structural Design Route of Phthalonitrile Resin," *Polymer* 210 (2020): 123001, https://doi.org/10.1016/j.polymer.2020.123001.

19. H. Zhu, M. Jia, Q. Li, C. Zhang, and P. Zheng, "Research the Effect of Crosslinking Degree on the Overall Performance of Novel Proton Exchange Membranes," *Solid State Ionics* 351 (2020): 115325, https://doi.org/10.1016/j.ssi.2020.115325.

20. W. Xu, G. Zhuang, Z. Chen, and J. Wei, "Experimental Study on the Micromorphology and Strength Formation Mechanism of Epoxy Asphalt During the Curing Reaction," *Applied Sciences* 10 (2020): 2610, https://doi.org/10.3390/app10072610.

21. Y. Liu, P. Ji, Z. Zhang, X. Yu, K. Naito, and Q. Zhang, "Synthesis and Properties of Pyrazine-Based Oligomeric Phthalonitrile Resins," *High Performance Polymers* 31 (2019): 1075–1084, https://doi.org/10.1177/0954008318823894.

22. G. Han, J. Hou, L. Wan, et al., "Enhance High-Temperature Mechanical Performance of a Silicon-Containing Arylether Arylacetylene Resin With the Aid of a Terminal Alkyne Compound," *Journal of Polymer Research* 28 (2021): 421, https://doi.org/10.1007/s10965-021-02775-9.

23. M. Ma, X. Liu, C. Li, Z. Qiao, Q. Yuan, and F. Huang, "Effects of Pendant Side Groups on the Properties of the Silicon-Containing Arylacetylene Resins With 2,5-Diphenyl-[1,3,4]-Oxadiazole Moieties," *RSC Advances* 11 (2021): 19656–19665, https://doi.org/10.1039/D1RA02184B.

24. R. J. Kern, "Preparation and Properties of Isomeric Polyphenylacetylenes," *Journal of Polymer Science Part A, Polymer Chemistry* 7 (1969): 621–631, https://doi.org/10.1002/pol.1969.150070216.

25. F. Zheng, K. Wan, F. Huang, et al., "Assessing Pyrolysis Behavior of Silicon-Containing Arylacetylene Resin via Experiments and ReaxFF MD Simulations," *Journal of Analytical and Applied Pyrolysis* 164 (2022): 105528, https://doi.org/10.1016/j.jaap.2022.105528.

26. A. Bondi, *Physical Properties of Molecular Crystals, Liquids, and Glasses*Journal of Polymer Science Part A-1: Polymer Chemistry (Wiley, 1968), SN 0449-296X.

27. J. He, L. Li, J. Zhou, et al., "Ultra-High Modulus Epoxy Resin Reinforced by Intensive Hydrogen Bond Network: From Design, Synthesis, Mechanism to Applications," *Composites Science and Technology* 231 (2023): 109815, https://doi.org/10.1016/j.compscitech.2022.109815.

28. M. Meador, M. Agnello, L. McCorkle, S. L. Vivod, and N. Wilmoth, "Moisture-Resistant Polyimide Aerogels Containing Propylene Oxide Links in the Backbone," *ACS Applied Materials & Interfaces* 8 (2016): 29073–29079, https://doi.org/10.1021/acsami.6b10248.

29. S. L. Vivod, M. A. B. Meador, C. Pugh, M. Wilkosz, K. Calomino, and L. McCorkle, "Toward Improved Optical Transparency of Polyimide Aerogels," *ACS Applied Materials & Interfaces* 12 (2020): 8622–8633, https://doi.org/10.1021/acsami.9b17796.

30. C. Qian, R. Bei, T. Zhu, et al., "Facile Strategy for Intrinsic Low-k Dielectric Polymers: Molecular Design Based on Secondary Relaxation Behavior," *Macromolecules* 52 (2019): 4601–4609, https://doi.org/10.1021/acs.macromol.9b00136.

31. N. Saba and M. Jawaid, "A Review on Thermomechanical Properties of Polymers and Fibers Reinforced Polymer Composites," *Journal of Industrial and Engineering Chemistry* 67 (2018): 1–11, https://doi.org/10.1016/j.jiec.2018.06.018.

32. X. Liu, S. Lv, K. Heng, et al., "Thermal and Thermoxidative Decomposition of a Heat-Resistant Poly(Dimethylsilylene Ethynylenephenyleneethynylene) Resin," *Journal of Thermal Analysis and Calorimetry* 148, no. 17 (2023): 8889–8901, https://doi.org/10.1007/s10973-023-12305-y.

Supporting Information

Additional supporting information can be found online in the Supporting Information section. **Data S1:** Supporting information.